NIH Public Access
Author Manuscript
J Biol Chem. Author manuscript; available in PMC 2006 May 26.

Published in final edited form as:
J Biol Chem. 2005 November 11; 280(45): 37461–37470.

Structural Analysis of Mg^{2+} and Ca^{2+} Binding to CaBP1, a Neuron-specific Regulator of Calcium Channels*

Jennifer N. Wingard[‡], **Jenny Chan**[§], **Ivan Bosanac**[§], **Françoise Haeseleer**[¶], **Krzysztof Palczewski**[¶,||,**,1], **Mitsuhiko Ikura**[§,2], and **James B. Ames**[‡,3]

‡*From the Center for Advanced Research in Biotechnology, University of Maryland Biotechnology Institute, Rockville, Maryland 20850*

§*From the Division of Signaling Biology, Ontario Cancer Institute and Department of Medical Biophysics, University of Toronto, Toronto, Ontario M5G 2M9, Canada*

¶*From the Department of Ophthalmology, University of Washington, Seattle, Washington 98195*

||*From the Department of Pharmacology, University of Washington, Seattle, Washington 98195*

***From the Department of Chemistry, University of Washington, Seattle, Washington 98195*

Abstract

CaBP1 (calcium-binding protein 1) is a 19.4-kDa protein of the EF-hand superfamily that modulates the activity of Ca^{2+} channels in the brain and retina. Here we present data from NMR, microcalorimetry, and other biophysical studies that characterize Ca^{2+} binding, Mg^{2+} binding, and structural properties of recombinant CaBP1 purified from *Escherichia coli*. Mg^{2+} binds constitutively to CaBP1 at EF-1 with an apparent dissociation constant (K_d) of 300 μM. Mg^{2+} binding to CaBP1 is enthalpic (ΔH = -3.725 kcal/mol) and promotes NMR spectral changes, indicative of a concerted Mg^{2+}-induced conformational change. Ca^{2+} binding to CaBP1 induces NMR spectral changes assigned to residues in EF-3 and EF-4, indicating localized Ca^{2+}-induced conformational changes at these sites. Ca^{2+} binds cooperatively to CaBP1 at EF-3 and EF-4 with an apparent K_d of 2.5 μM and a Hill coefficient of 1.3. Ca^{2+} binds to EF-1 with low affinity (K_d >100 μM), and no Ca^{2+} binding was detected at EF-2. In the absence of Mg^{2+} and Ca^{2+}, CaBP1 forms a flexible molten globule-like structure. Mg^{2+} and Ca^{2+} induce distinct conformational changes resulting in protein dimerization and markedly increased folding stability. The unfolding temperatures are 53, 74, and 76 °C for apo-, Mg^{2+}-bound, and Ca^{2+}-bound CaBP1, respectively. Together, our results suggest that CaBP1 switches between structurally distinct Mg^{2+}-bound and Ca^{2+}-bound states in response to Ca^{2+} signaling. Both conformational states may serve to modulate the activity of Ca^{2+} channel targets.

A family of neuronal calcium-binding proteins (CaBP[4]1-5 (1,2)), similar in sequence to calmodulin, represents a new sub-branch of the EF-hand superfamily (3-5). CaBPs are vertebrate-specific proteins expressed predominantly in the brain and retina. Multiple splice variants and various isoforms of CaBPs have been identified and localized in different neuronal cell types (6-9). The abundance and multiplicity of CaBPs in the central nervous system suggest a role in signal transduction. Indeed, it was recently discovered that CaBP1, also termed caldendrin (10), modulates the Ca^{2+}-sensitive activity of inositol 1,4,5-trisphosphate receptors

*This work was supported in part by Grants EY012347 and NS045909 (to J. B. A.) and EY08061 (to K. P.) from the National Institutes of Health. The costs of publication of this article were defrayed in part by the payment of page charges. This article must therefore be hereby marked "*advertisement*" in accordance with 18 U.S.C. Section 1734 solely to indicate this fact.

[3]To whom correspondence should be addressed: Center for Advanced Research in Biotechnology, Rockville, MD 20850. Tel.: 240-314-6120; Fax: 240-314-6255; E-mail: james@carb.nist.gov.
[1]Present address: Dept. of Pharmacology, School of Medicine, Case Western Reserve University, Cleveland, OH 44106-4965.
[2]Supported by Canadian Institutes of Health Research and holds Canada Research Chair in Cancer Structural Biology.

NIH-PA Author Manuscript
NIH-PA Author Manuscript
NIH-PA Author Manuscript

NIH-PA Author Manuscript

NIH-PA Author Manuscript

NIH-PA Author Manuscript

($InsP_3Rs$) that serve as Ca^{2+} release channels on the endoplasmic reticulum membrane (11, 12). CaBP1 also interacts with P/Q-type voltage-gated Ca^{2+} channels (13), L-type channels (14,15), and the transient receptor potential channel, TRPC5 (16). CaBP4 has been shown to regulate Ca^{2+}-dependent voltage gating of L-type Ca^{2+} channels in the retina (17). Thus, the CaBP proteins are emerging as a family of calcium sensors that modulate the activity of multiple neuronal Ca^{2+} channels.

CaBP proteins each contain four EF-hands, similar in sequence to those found in calmodulin and troponin C (3,4) (Fig. 1). By analogy to the structure of calmodulin (18), the four EF-hands of CaBP proteins are believed to form an N-terminal domain composed of EF-1 and EF-2 and a C-terminal domain composed of EF-3 and EF-4. The two domains are connected by a central linker that is four residues longer in CaBPs than in calmodulin. The extra residues in the linker may extend a “central helix” by one turn, generating an elongated structure similar to calmodulin. Alternatively, the extra residues might form a U-shaped linker that promotes interdomain association similar to that found in recoverin (5,19,20) and other members of the neuronal calcium sensor protein family (21-26). In contrast to calmodulin, the CaBPs contain a variable stretch of nonconserved amino acids within the N-terminal region. The variable N-terminal residues of CaBPs are generated in part by splice variants of CaBP1 and CaBP2 (see the *italicized* residues in Fig. 1). The N-terminal sequence variability is likely to confer target specificity. Another distinguishing property of the CaBPs is that the second EF-hand lacks critical residues required for high affinity Ca^{2+} binding. A conserved glycine at the 5-position of the loop in EF-2 (*e.g.* Gly-75 in CaBP1) cannot chelate Ca^{2+} and therefore would be expected to disable physiological Ca^{2+} binding to EF-2. By contrast, EF-2 of calmodulin contains asparagine at the 5-position, which promotes high affinity Ca^{2+} binding at this site (18,27).

In CaBP1 and CaBP5, the first EF-hand (EF-1) contains aspartate (*e.g.* Asp-46 in CaBP1) instead of the usual glutamate at the 12-position of the EF-hand binding loop (Fig. 1). This substitution in other EF-hand proteins is known to diminish binding selectivity of Ca^{2+} *versus* Mg^{2+} (28-30). Mg^{2+} binding to the first EF-hand of CaBP1 or CaBP5 might be sufficient

---

[4]The abbreviations used are:

CaBP calcium-binding protein

DTT dithiothreitol

$InsP_3Rs$ inositol 1,4,5-trisphosphate receptors

DLS dynamic light scattering

DSC differential scanning calorimetry

HSQC heteronuclear single quantum coherence

ITC isothermal titration calorimetry

SEC size exclusion chromatography

SLS static light scattering

CaM calmodulin

NIH-PA Author Manuscript

NIH-PA Author Manuscript

NIH-PA Author Manuscript

to drive functional protein conformational changes. Magnesium is not normally considered a regulator, but recent *in vivo* measurements have detected changes in free Mg^{2+} concentrations in cortical neurons after treatment with neurotransmitter (31). Other neuronal calcium-binding proteins such as DREAM (29), GCAP2 (32), and neuronal calcium sensor-1 (33) also bind Mg^{2+} and exhibit Mg^{2+}-induced physiological effects. Therefore, it is of interest to investigate the structure and function of Mg^{2+} binding to CaBPs.

Here we present a structural analysis of Mg^{2+} and Ca^{2+} binding to the individual EF-hands in CaBP1. The results reveal that EF-1 binds constitutively to Mg^{2+}; EF-2 does not bind Ca^{2+} or Mg^{2+}; EF-3 and EF-4 bind functionally to Ca^{2+}; and both Mg^{2+} and Ca^{2+} promote protein dimerization and increase folding stability. These results serve as a prelude to future structural analyses that will determine at atomic resolution the Ca^{2+}-induced conformational changes of CaBPs in order to understand their Ca^{2+}-sensitive regulation of physiological target proteins.

EXPERIMENTAL PROCEDURES

Expression and Purification of Human CaBP1—All experiments in this study were performed on a small splice variant of human CaBP1, previously termed s-CaBP1 (1) and referred to in this study as CaBP1. *Escherichia coli* strain BL21 (DE3), transformed with plasmid pET15b-CaBP1, was grown in LB broth (containing 100 μg/ml ampicillin) at 37 °C until the A_{600nm} reached ~1.0 and then was diluted 1:50 in LB and grown again at 37 °C. At A_{600nm} = 0.5, CaBP1 expression was induced with 0.5 mM isopropyl 1-thio-β-D-galactopyranoside. After a 3-h induction period, the cells were harvested by centrifugation. The cell pellet was then suspended in Lysis Buffer containing 20 mM Tris, 0.1 M KCl, 1 mM EGTA, 1 mM dithiothreitol, and 10% glycerol, pH 7.5, and flash-frozen using liquid nitrogen. Frozen aliquots were stored at -70 °C. Thawed cells with 0.1 mM phenylmethylsulfonyl fluoride were disrupted via sonication using a Branson Sonifier 450 at 50% duty cycle, output 4-5 on ice, for 2 min with two repetitions and a 2-min cooling period in between. CaBP1 was recovered by ultracentrifugation at 35,000 rpm for 1 h at 4°C. The supernatant, supplemented with 4 mM $CaCl_2$ and 0.2 M KCl, was passed through a phenyl-Sepharose column (Amersham Biosciences), washed for 6 column volumes, and eluted with a 200-min gradient elution in a low salt buffer containing 50 mM KCl and 2 mM EGTA. Fractions containing protein were visualized by Coomassie-stained SDS-polyacrylamide gels. Selected fractions were then pooled, diluted 1:3 with an equilibration buffer (20 mM Tris, 2 mM EGTA, 1 mM dithiothreitol, pH 7.5), and further purified using a Q HP-Sepharose column (Amersham Biosciences) at room temperature using a 200-min gradient elution. Fractions containing pure CaBP1 as visualized by Coomassie-stained SDS-polyacrylamide gels were pooled and concentrated using Amicon Ultra 15 centrifugal filters (Millipore) with a 10-kDa molecular mass cut-off. The overall yield was ~16 mg of protein from 1 liter of cell culture. The protein concentration was determined by measuring the A_{280nm} and a molar absorption coefficient of $\epsilon = 3960\ M^{-1}\ cm^{1-}$.

Preparation of ApoCaBP1 and Mg^{2+}-bound CaBP1 for Ca^{2+} Binding Studies—ApoCaBP1 was prepared by adding 5 mM EGTA to purified material in a pre-rinsed Amicon filter. The CaBP1 was then concentrated to 1 ml and washed with 15 ml of Ca^{2+}-free, Mg^{2+}-free buffer. The washes were repeated five times until remaining EGTA was negligible (<1 nM). Mg^{2+}-bound CaBP1 was prepared similarly but was washed with a buffer containing Mg^{2+}. All glassware and tubes that contacted apo- or Mg^{2+}-bound CaBP1 were first washed with 0.1 M HCl, followed by multiple rinses with decalcified buffer.

Binding of $^{45}Ca^{2+}$—$^{45}Ca^{2+}$ radioactive isotope (calcium-45, calcium chloride in aqueous solution, specific activity = 850 mCi/ml; Amersham Biosciences) was used to quantitate the binding of Ca^{2+} to CaBP1. $^{45}Ca^{2+}$ binding to CaBP1 was measured as the protein-bound radioactivity retained after ultrafiltration using a procedure described previously (34) based on

NIH-PA Author Manuscript

NIH-PA Author Manuscript

NIH-PA Author Manuscript

the original method of Paulus (35). The buffer used in the Ca^{2+} titration (20 mM Tris-HCl, 0.1 M KCl, 1 mM dithiothreitol, pH 7.5) and protein samples were decalcified by treatment with Chelex resin (Bio-Rad). A Centricon-10 concentrator (10-kDa cut-off, 2-ml sample compartment; Millipore Corp.) used in the titration was pretreated to remove contaminating Ca^{2+}. The lower chamber was rinsed with 0.1 M HCl, followed by several rinses with decalcified buffer. The concentrator membrane was decalcified by rinsing with 5% $NaHCO_3$ followed by several rinses with decalcified buffer. A decalcified protein sample (1.5 ml, 80 μM) was placed into the sample compartment, and 12 μl of 0.25 mM $^{45}Ca^{2+}$ solution (2.6 μCi) was added. The sample was carefully mixed and centrifuged (2300 rpm, 2 min) by using a tabletop centrifuge (Beckman model TJ-6), forming 25 μl of filtrate. The filtrate was returned to the sample chamber, mixed, and centrifuged a second time to minimize any dead volume. The radioactivity of 10 μl of the filtrate (proportional to the free Ca^{2+} concentration) and radioactivity of an equal volume of the protein sample (proportional to total Ca^{2+} concentration) were separately measured by liquid scintillation counting (Liquid Scintillation Analyzer, Packard Instrument Co.). Aliquots of nonradioactive Ca^{2+} were added serially to the protein sample to adjust the total Ca^{2+} concentration throughout the titration (2, 15, 29, 56, 83, 112, 140, 197, 255, 313, 458, and 605 μM). The corresponding radioactivities of filtrate and protein sample were measured for each point in the titration. The free and bound Ca^{2+} concentrations at each point in the titration were calculated from the measured radioactivity as described previously (36), and fractional saturation was plotted as a function of free Ca^{2+} concentration (Fig. 2).

Differential Scanning Calorimetry—DSC experiments were performed using a MicroCal VP-DSC microcalorimeter as described previously (37). Samples of apoCaBP1 were prepared as for the Ca^{2+} binding studies. Aliquots of the apoCaBP1 were dialyzed overnight in buffer supplemented with 5 mM EGTA (apo-), 5 mM $MgCl_2$ (Mg^{2+}-bound), or 5 mM $CaCl_2$ (Ca^{2+}-bound) using Pierce Slide-a-lyzer minidialysis units, 3.5-kDa molecular mass cut-off. The buffer consisted of 20 mM Tris, pH 7.5, 100 mM NaCl, and 1 mM DTT. Samples of 126 μM CaBP1 were heated in a MicroCal VP-DSC calorimeter in a 10-120 °C range at a scan rate of 60 °C/h, then cooled, and rescanned to check for thermal transition reversibility. Samples were also scanned at slower scan rates in order to examine resolution of any peak shoulders. A buffer scan was subtracted from each data set to correct for base-line error. Data analysis was performed using the EXAM program (37).

Isothermal Titration Calorimetry—ITC experiments were performed using a MicroCal VP-ITC microcalorimeter as described previously (29). Samples of apoCaBP1 were prepared as described for the Ca^{2+} binding studies, and apoCaBP1 was dialyzed against decalcified buffer overnight. A sample of the dialysis buffer was placed in the reference cell, and samples of apo- or Mg^{2+}-bound CaBP1 were placed in the sample cell. Experiments were performed at 25 °C and with protein concentrations between 120 and 180 μM. 40 injections of 15 mM $MgCl_2$ or 5 mM $CaCl_2$, prepared using decalcified buffer, were made in 5-μl aliquots. An injection delay of 240 s was utilized to allow for the base line to return after each injection. A titration into dialysis buffer was subtracted from the data to correct for heat of dilution. For each addition of ligand, the molar heat (Q_t) was measured as a function of total ligand concentration (X_t) as shown in Equation 1,

$$Q_t = n \cdot M_t \cdot \Delta H \cdot V\left\{1 + X_t / \left(n \cdot M_t\right) + 1 / \left(n \cdot K_a \cdot M_t\right) - \left[\left(1 + X_t / \left(n \cdot M_t\right) + 1 / \left(n \cdot K_a \cdot M_t\right)\right)^2 - 4X_t / \left(n^* M_t\right)\right]^{0.5}\right\} / 2 \quad \text{(Eq.1)}$$

where n is the number of sites; M_t is the total protein monomer concentration; K_a is the metal-binding association constant ($1/K_d$), and V is the cell volume. The differential heat (dQ_t) was fit to various kinetic models (sequential and independent sites) by using a nonlinear least squares minimization method (38,39) performed using MicroCal Origin ITC software. Thermodynamic parameters in the analysis were defined as shown in Equation 2,

NIH-PA Author Manuscript

NIH-PA Author Manuscript

NIH-PA Author Manuscript

$$\Delta G = \Delta H - T\Delta S \quad \text{(Eq.2)}$$

and

$$\Delta G = -nRT\ln(K_a) \quad \text{(Eq.3)}$$

where n is the number of moles; T is the absolute temperature, and R is 8.3151 J mol^{-1} K^{-1}.

Gel Filtration Size Exclusion Chromatography—Size exclusion chromatography experiments were performed on CaBP1 in buffer containing 20 mM Tris, pH 7.5, 0.1 M KCl, 1 mM DTT with the addition of either 2 mM EGTA (apo-), 2 mM EGTA + 1 mM $MgCl_2$ (Mg^{2+}-bound), or 2 mM $CaCl_2$ (Ca^{2+}-bound). 250 μl of each sample/standard was freshly prepared, injected, and eluted on a Superdex 200 column (Amersham Biosciences) via the AKTA Prime (Amersham Biosciences) at a flow rate of 0.4 ml/min at room temperature. To run successfully at such a low flow rate, all air bubbles were purged before each run according to the manufacturer's instructions. The protein standards used in the analysis were β-amylase (200 kDa), alcohol dehydrogenase (150 kDa), albumin (66 kDa), carbonic anhydrase (29 kDa), and cytochrome *c* (12.4 kDa). The elution volume (V_e) of each protein was monitored separately at 280 nm. Dextran blue was injected and used to determine the column void volume (V_o). The molecular mass of CaBP1 was extrapolated from a standard curve of V_e/V_o *versus* molecular mass on a semilog scale. Experiments were repeated twice to ensure consistency and accuracy.

Static Light Scattering—Static light scattering experiments were performed using a Zetasizer Nano S (Malvern Instruments). CaBP1 samples were filtered with a 0.02-μm Anotop 10 filter (Whatman). Measurements were performed at 25 °C in a buffer containing 20 mM Tris, pH 7.5, 100 mM KCl, and 1 mM tris(2-carboxyethyl)phosphine supplemented with either 2 mM EGTA (apo-), 5 mM $MgCl_2$ (Mg^{2+}-bound), or 2 mM $CaCl_2$ (Ca^{2+}-bound). SLS measurements were made using serial dilutions of CaBP1 (3 to 0.75 mg/ml). The average molecular mass of CaBP1 in solution was determined from analysis of a Debye plot of the light scattering as described previously (40). Toluene served as a standard reference, and a differential refractive index (d*n*/d*c*) of 0.185 ml/g was used in the analysis. Data were analyzed using the Zetasizer Nano software provided with the instrument.

Dynamic Light Scattering—DLS experiments were performed on filtered samples of CaBP1 (described above) at 25 °C using a Zetasizer Nano S instrument (Malvern Instruments). Multiple experimental runs were performed to ensure accuracy. Time-correlated fluctuations in light scattering caused by Brownian motion of CaBP1 were analyzed by an autocorrelator inside the DLS instrument and modeled by the first-order autocorrelation function as described previously (40). The translational diffusion coefficient (D_t) of CaBP1 derived from this analysis was then used to calculate the hydrodynamic radius (R_H) using the Stokes-Einstein equation, $D_t = k_B T/6\pi\eta R_H$, where k_B is Boltzmann constant; T is temperature in Kelvin; η is solvent viscosity, and R_H is the hydrodynamic radius of CaBP1.

NMR Spectroscopy—Samples for NMR analysis were prepared by dissolving ^{15}N-labeled CaBP1 (0.5 mM) in 0.3 ml of a 95% H_2O, 5% $[^2H]H_2O$ solution containing 10 mM $[^2H_{11}]$Tris, pH 7.4, 5 mM $[^2H_{10}]$tris(2-carboxyethyl)phosphine, 0.1 M KCl, and either 5 mM EDTA (apo-), 5 mM $MgCl_2$ (Mg^{2+}-bound), or 10 mM $CaCl_2$ + 5 mM $MgCl_2$ (Ca^{2+}-bound). All NMR experiments were performed at 30 °C on a Bruker Avance 600 MHz spectrometer equipped with a four-channel interface and triple resonance probe with triple axis pulsed field gradients. The ^{15}N-^1H HSQC spectra (see Fig. 7) were recorded on samples of ^{15}N-labeled CaBP1 (in 95% H_2O, 5% ^2H_2O). The number of complex points and acquisition times were 256, 180 ms ($^{15}N(F_1)$), and 512, 64 ms (^1H (F_2)). Partial sequence-specific resonance assignments were obtained as described previously (41).

NIH-PA Author Manuscript

NIH-PA Author Manuscript

NIH-PA Author Manuscript

RESULTS

Equilibrium $^{45}Ca^{2+}$ Binding Measurements—CaBP1 contains four EF-hand Ca^{2+}-binding motifs (Fig. 1). The second EF-hand (EF-2) contains Gly-75 at the 5-position of the EF-hand loop that should preclude Ca^{2+} binding. The remaining EF-hands in CaBP1 (EF-1, EF-3, and EF-4) match the consensus and were expected to bind Ca^{2+}. To quantitate the number of ions that bind to CaBP1 at saturation, direct measurements of $^{45}Ca^{2+}$ binding were performed on samples of recombinant CaBP1 purified from *E. coli* (Fig. 2). At least two Ca^{2+} bind to the protein with relatively high affinity at physiological Ca^{2+} concentrations (0.1-20 μM), and a third Ca^{2+} appears to bind with much lower affinity at Ca^{2+} concentrations beyond 100 μM. The binding of three Ca^{2+} to CaBP1 at saturation (Fig. 2) is consistent with the view that EF-2 is disabled, whereas EF-1, EF-3, and EF-4 are functional. However, the relatively high uncertainty of the $^{45}Ca^{2+}$ binding data at higher Ca^{2+} concentrations in the titration (>100 μM), due to nonspecific binding of Ca^{2+} and other experimental artifacts, precluded a quantitative description of the low affinity site in the analysis below.

The fractional saturation (*Y*), computed from the $^{45}Ca^{2+}$ binding data, can be represented by the Hill equation as shown in Equation 4,

$$Y = \frac{\left[Ca^{2+}\right]^a}{\left[Ca^{2+}\right]^a + K_d^a} \quad \text{(Eq. 4)}$$

where $[Ca^{2+}]$ is the free Ca^{2+} concentration; K_d is the apparent dissociation constant, and *a* denotes the Hill coefficient. The fractional saturation data for CaBP1 (Fig. 2), at physiological Ca^{2+} concentrations (0.1-30 μM), is best fit by the Hill equation using the parameters K_d = 2.5 μM and *a* = 1.3 (see *dotted line* in Fig. 2). A Hill coefficient greater than 1 in this case suggests that two Ca^{2+} bind to the protein in the physiological range with positive cooperativity, suggesting that the two physiological sites are likely EF-3 and EF-4, as they interact structurally with one another in the C-terminal domain of CaBP1. This implies that the low affinity site is EF-1, consistent with the NMR analysis below. The presence of Asp-46 (instead of Glu) at the 12-position of EF-1 may explain the unusually low Ca^{2+} affinity of EF-1.

The $^{45}Ca^{2+}$ binding assay was also conducted on CaBP1 in the presence of physiological Mg^{2+} concentrations (5 mM). The fractional saturation data for CaBP1 in the physiological range of Ca^{2+} and the presence of Mg^{2+} (*open circles* in Fig. 2) is best fit to the Hill equation using the parameters K_d = 3 μM and *a* = 1.3, indicating that Mg^{2+} has only a minor effect on Ca^{2+} binding to the two high affinity sites (EF-3 and EF-4). By contrast, Ca^{2+} binding to the low affinity site (EF-1) was less apparent in the presence of Mg^{2+}, suggesting that EF-1 might be constitutively occupied by Mg^{2+} under physiological conditions (0.1-10 μM Ca^{2+} and 5 mM Mg^{2+}).

Energetics of Ca^{2+} and Mg^{2+} Binding—The energetics of Ca^{2+} and Mg^{2+} binding to CaBP1 were measured using isothermal titration calorimetry (ITC, see Equations 1-3). Intrinsic metal binding to proteins is usually entropically driven ($\Delta H > 0$) because of the high dehydration enthalpies of divalent cations (42). However, the overall enthalpy of divalent cation binding to a protein can be exothermic ($\Delta H < 0$) if it is thermodynamically coupled to enthalpic equilibria such as a protein conformational change (43).

Titration of $CaCl_2$ into apoCaBP1 (in the absence of Mg^{2+}) resulted in a multiphasic calorimetric Ca^{2+} binding isotherm that could be fit by the binding of 2 or more Ca^{2+} ions (Fig. 3*A*). The ITC isotherm exhibits an initial endothermic phase (K_d ~2.5 μM and ΔH = +0.7 kcal/mol) representing stoichiometric binding of one Ca^{2+}, to the protein, followed by an exothermic phase, representing subsequent binding of multiple Ca^{2+} ions. The exothermic phase likely

NIH-PA Author Manuscript

NIH-PA Author Manuscript

NIH-PA Author Manuscript

represents the binding of two Ca^{2+} to the protein because the negative enthalpy observed in the latter part of the titration persists until a Ca^{2+}/protein ratio of 3 is reached, and declines substantially thereafter.

The ITC Ca^{2+} binding isotherm was also measured in the presence of physiological Mg^{2+} (Fig. 3*B*). In this case, the isotherm exhibits an initial endothermic phase (K_d~2.5 μM and ΔH =+0.61 kcal/mol), representing stoichiometric Ca^{2+} binding to a high affinity site, followed by exothermic binding to a lower affinity site (K_d~20 μM and ΔH = -0.53 kcal/mol). The endothermic Ca^{2+} binding appears insensitive to Mg^{2+}. The exothermic Ca^{2+} binding, by contrast, is much more responsive to Mg^{2+}, and the apparent negative amplitude of the isotherm is much shallower in the presence of saturating Mg^{2+} than it is in the absence of Mg^{2+}. As a consequence, the exothermic phase represents binding of just one Ca^{2+} to the protein in the presence of Mg^{2+} (Fig. 3*B*), in contrast to at least two sites in the absence of Mg^{2+} (Fig. 3*A*). In summary, the ITC analysis indicates that a total of three Ca^{2+} bind to the protein in the absence of Mg^{2+} (Fig. 3*A*) and only two Ca^{2+} bind to CaBP1 in the presence of a physiological level of Mg^{2+}(Fig. 3*B*). The ITC results are consistent with constitutive Mg^{2+} binding at EF-1 under physiological conditions as suggested above by the $^{45}Ca^{2+}$ binding data (Fig. 2) and NMR analysis (below).

The effect of Mg^{2+} on the Ca^{2+} binding isotherm (Fig. 3) prompted us to quantitate the Mg^{2+} binding properties of CaBP1 using ITC. Titration of $MgCl_2$ into apoCaBP1 resulted in a simple monophasic isotherm (Fig. 4). Analysis of the Mg^{2+} binding isotherm using a "1-site" model (Microcal Origin software) revealed that at least one Mg^{2+} binds enthalpically to CaBP1 with modest affinity (dissociation constant of 300 μM and ΔH =-3.7 kcal/mol). Intrinsic Mg^{2+} binding to most proteins is usually entropically driven (30). The enthalpic binding of Mg^{2+} to CaBP1 suggests a possible Mg^{2+}-induced conformational change. NMR spectra of CaBP1 and protein folding stability change quite dramatically upon the addition of saturating Mg^{2+} (see below), suggesting that Mg^{2+} binding stabilizes the tertiary structure of CaBP1.

Mg^{2+} and Ca^{2+} Stabilize Protein Folding—DSC experiments were performed on CaBP1 to assess quantitatively the effect of Ca^{2+} and Mg^{2+} on protein folding stability. Representative DSC scans of CaBP1 are shown in Fig. 5*A*. The peak maximum of apoCaBP1 (transition temperature, T_m = 53 °C) is almost 20 °C lower than the peak maxima of both Mg^{2+}-bound (T_m = 74 °C) and Ca^{2+}-bound (T_m = 76 °C) CaBP1, indicating that both Mg^{2+} and Ca^{2+} increase the folding stability to nearly the same extent. The transition peaks did not fully reappear upon re-scanning each of the samples, suggesting irreversible unfolding due to aggregation and/or denaturation. However, the post-transitional base line and T_m in each case were independent of protein concentration and scan rate, consistent with a two-state model of unfolding. The DSC thermogram of apoCaBP1 is broad with at least two transitions and could not be fit by a two-state model. By contrast, the DSC thermograms for both Mg^{2+}-bound and Ca^{2+}-bound forms of CaBP1 each exhibit a sharp transition peak, suggesting that unfolding takes place in one cooperative step. A sharp one-step folding transition suggests that the two predicted domains of CaBP1 may be structurally associated with each other, in contrast to the independently folded domains of calmodulin (44-46). The DSC thermograms for Mg^{2+}-bound and Ca^{2+}-bound CaBP1 were optimally fit by the two-state model, B → 2A, where B and A represent the folded and unfolded states, respectively (Fig. 5, *B* and *C*). The optimal fitting parameters were T_m = 76.6 °C and ΔH_v = 287 cal/mol for Mg^{2+}-bound CaBP1, and T_m = 76.8 °C and ΔH_v = 341 cal/mol for Ca^{2+}-bound CaBP1. The fits were markedly worse using the simpler model, B → A, where the folded state is a monomer. The robust precision of the fit to the dimer model (B → 2A) strongly suggests that both Mg^{2+}-bound and Ca^{2+}-bound forms of CaBP1 exist as a dimer in the folded state. These results are in contrast with that of calmodulin (45-47) and related EF-hand proteins such as CIB (30), which exhibit a monomeric folded state and significantly lower T_m for the Mg^{2+}-bound protein.

NIH-PA Author Manuscript

NIH-PA Author Manuscript

NIH-PA Author Manuscript

Hydrodynamic Analysis of CaBP1 Dimerization—Dynamic light scattering (DLS), static light scattering (SLS), and size exclusion chromatography (SEC) experiments were performed on CaBP1 to estimate the hydrodynamic radius and oligomerization state of the protein in solution. Static light scattering (SLS) measurements determined an average protein mass of 20.6 kDa for apoCaBP1, similar to the theoretical mass of the CaBP1 polypeptide (19.4 kDa). By contrast, the protein masses of Mg^{2+}-bound (40.54 kDa) and Ca^{2+}-bound (38.78 kDa) CaBP1 as determined by SLS suggest protein dimer formation. The second virial coefficient (A_2) calculated from the SLS data were positive for Mg^{2+}-bound CaBP1, suggesting moderate solubility, whereas negative A_2 values for both apo- and Ca^{2+}-bound CaBP1 indicated a tendency toward aggregation. The SEC elution volumes, calibrated against spherical protein standards, corresponded to molecular masses of 32, 28, and 27 kDa for apo-, Mg^{2+}-bound, and Ca^{2+}-bound CaBP1, respectively. Similar protein masses were also derived from glycerol gradient diffusion experiments (data not shown). The disparity in protein masses derived from SEC and SLS studies might be explained in part by calibration differences. The SEC standard curve was calibrated using highly spherical protein standards with similar charge densities. CaBP1, however, may have an elongated or otherwise nonspherical shape with internal flexibility like that of calmodulin (48). Therefore, the SLS analysis, employing a cylindrical shape model, may determine a more accurate protein mass in this case. Translational diffusion properties of CaBP1 measured by DLS provided an additional and independent measure of protein mass. The hydrodynamic radius (R_H) of CaBP1 measured by DLS was somewhat variable with a broad size distribution (Fig. 6). The DLS size histograms showed polydispersities of 40, 20, and 25% for apo-, Mg^{2+}-bound, and Ca^{2+}-bound CaBP1, respectively, suggesting a heterogeneous population of protein species. The polydispersity suggests that CaBP1 may exhibit conformational heterogeneity or exist as an equilibrium mixture of monomer and dimer species. The SLS and DSC analyses stated above argue in favor of protein dimerization for the Mg^{2+}-bound and Ca^{2+}-bound forms of CaBP1. Consistent with this view, the hydrodynamic radii of both Mg^{2+}- and Ca^{2+}-bound forms of CaBP1 increase as a function of protein concentration measured below by pulsed-field gradient diffusion NMR studies. In summary, the hydrodynamic properties measured independently by SEC, DLS, and NMR suggest that CaBP1 forms a dynamic and relatively low affinity protein dimer in solution.

Mg^{2+} and Ca^{2+} Stabilize Tertiary Structure of CaBP1—NMR spectroscopy was used to probe protein conformational changes in CaBP1 induced by Mg^{2+} and/or Ca^{2+} binding (Fig. 7). The peaks in the ^{1}H-^{15}N HSQC NMR spectra represent main chain and side chain amide groups and provide a residue-specific fingerprint of the overall protein conformation. The two-dimensional ^{1}H-^{15}H HSQC spectrum of apoCaBP1 exhibited poorly resolved and overlapping peaks with narrow chemical shift dispersion in the amide proton dimension (Fig. 7, *left panel*). The number of observed peaks was less than the expected number of amide groups (132 peaks *versus* 167 residues), and the intensities of many peaks were quite weak, perhaps due to exchange broadening caused by dimerization or conformational heterogeneity. The poor chemical shift dispersion suggests that apoCaBP1 adopts an unstructured molten-globule state similar to that described for the apo states of many other Ca^{2+}-binding proteins such as GCAP-2 (21), Frq1 (22), CIB (30), calexcitin (49), protein S (50), and DREAM (29). However, circular dichroism analysis (data not shown) suggests that apoCaBP1 adopts a high degree of helical content, consistent with the formation of the four EF-hands, and that the helical content does not change much upon binding Mg^{2+} and/or Ca^{2+}. Together, our structural studies suggest that apoCaBP1 adopts a native secondary structure but is in a flexible molten-globule state.

The HSQC spectrum of CaBP1 changed dramatically upon the addition of saturating Mg^{2+} (Fig. 7, *middle panel*). Mg^{2+} caused a greater number of peaks to appear (155 peaks *versus* 167 residues), and the NMR intensities were in general much more uniform than those of apoCaBP1. Mg^{2+} binding to CaBP1 substantially improved the NMR chemical shift dispersion and markedly increased the number of observable long range nuclear Overhauser effects,

NIH-PA Author Manuscript

NIH-PA Author Manuscript

NIH-PA Author Manuscript

demonstrating that Mg^{2+}-bound CaBP1 adopts a stable tertiary structure. Two downfield-shifted peaks appeared (assigned as Gly-40 and Gly-117) that are characteristic of conserved glycine residues at the 6-position of divalent metal occupied EF-hands and suggest that Mg^{2+} is bound at EF-1 and EF-3. The average peak width in the spectrum appears broader than expected for a monomeric protein, consistent with protein dimerization described above. Pulsed-field gradient diffusion NMR studies (51) determined a hydrodynamic radius of 2.7 nm (corresponding to a spherical molecular mass of 34 kDa) for Mg^{2+}-bound CaBP1 at 500 μ_M protein concentration, consistent with mostly dimer species present under conditions for NMR.

The HSQC spectrum of CaBP1 changed even further upon the addition of saturating Ca^{2+} (Fig. 7, *right panel*). Significant spectral changes induced by the addition of saturating Ca^{2+} to the Mg^{2+}-bound protein sample indicated that Ca^{2+}-induced conformational changes are distinct and separate from the Mg^{2+}-induced changes (Fig. 7, *middle* and *right panels*). Three downfield-shifted peaks near 10.5 ppm are characteristic of conserved glycine residues at the 6-position of Ca^{2+}-occupied EF-hands (Gly-40, Gly-117, and Gly-154), consistent with Ca^{2+} bound at EF-1, EF-3, and EF-4. Additional unique peaks of Ca^{2+}-bound CaBP1 (observed between 9 and 10 ppm) represent amino acid in residues EF-1, EF-3, and EF-4 altered structurally Ca^{2+} binding. The spectrum of Ca^{2+} by HSQC-saturated CaBP1 exhibited somewhat broadened peaks (like that of Mg^{2+}-bound protein) with variable NMR intensities, consistent with protein dimerization. Pulsed-field gradient diffusion NMR studies determined a hydrodynamic radius of 2.8 nm, corresponding to a Ca^{2+}-bound protein dimer.

Kinetic Structural Changes Probed by NMR—NMR spectra of CaBP1 were analyzed to probe kinetic structural changes at specific amino acid locations within the protein as a function of Mg^{2+} and/or Ca^{2+} (Figs. 8-10). The Mg^{2+}- and Ca^{2+}-induced spectral changes reflect mostly slow exchange processes on the chemical shift time scale, consistent with high affinity metal binding. The NMR intensities of representative amide resonances assigned to Gly-40 (EF-1), Val-78 (EF-2), Gly-117 (EF-3), and Gly137 (EF-4) are plotted as a function of Mg^{2+} concentration (Fig. 8*A*). These resonances (as well as many others assigned to Mg^{2+}-bound CaBP1) increase monotonically in intensity as a function of adding up to 2 eq of Mg^{2+} per protein. After adding 2 or more eq of Mg^{2+}, no further intensity change occurred, suggesting that two Mg^{2+} bind to CaBP1 at saturation. The Mg^{2+}-induced spectral changes from residues in all four EF-hands suggest that Mg^{2+} binding induces a global and concerted conformational change throughout the protein.

Amide NMR intensities of residues Ser-120 (EF-3) and Leu-150 (EF-4) are plotted as a function of Ca^{2+} concentration (Fig. 8*B*). These resonances (as well as others assigned to residues of EF-3 and EF-4 of Ca^{2+}-bound CaBP1) increase monotonically in intensity as a function of Ca^{2+} up to 2 eq. After adding 2 or more eq of Ca^{2+}, no further intensity change was detected, suggesting that two Ca^{2+} bind to CaBP1 in the presence of physiological levels of excess Mg^{2+} (5 m_M). The Ca^{2+}-induced spectral changes exhibited by residues in both EF-3 (Ser-120) and EF-4 (Leu-150) suggested that Ca^{2+} induces a protein conformational change in EF-3 and EF-4. By contrast, amide resonances assigned to residues of EF-1 and EF-2 did not exhibit significant Ca^{2+}-induced spectral changes in the presence of physiological Mg^{2+} (data not shown), suggesting that EF-1 and EF-2 do not bind Ca^{2+} in the presence of excess Mg^{2+} and that the N-terminal domain does not change structure upon Ca^{2+} binding to EF-3 and EF-4.

Downfield-shifted amide proton chemical shifts (~10-11 ppm) of conserved glycine residues at the 6-position of EF-hands generally are characteristic of divalent metal binding at these sites (Fig. 9). Amide proton chemical shifts observed for Gly-40 (10.38 ppm) and Gly-117 (10.58 ppm) of Mg^{2+}-bound CaBP1 (Fig. 7, *middle panel*, and Fig. 9*A*) indicate that Mg^{2+} is

NIH-PA Author Manuscript

NIH-PA Author Manuscript

NIH-PA Author Manuscript

bound at EF-1 and EF-3. The addition of 1 eq of Ca^{2+} to the protein causes severe broadening of the downfield peak at 10.58 ppm (Gly-117), whereas the peak at 10.38 ppm (Gly-40) remains relatively unchanged (Fig. 9*B*). Further addition of Ca^{2+} causes a new downfield peak to appear at 10.41 ppm (assigned to Gly-117), indicative of Ca^{2+} binding at EF-3 (Fig. 9*C*). A shoulder peak at 10.45 ppm (assigned to Gly-154) is indicative of Ca^{2+} binding at EF-4 (Fig. 9, *C-F*). The downfield peak at 10.38 ppm (Gly-40) persists although the Ca^{2+}/Mg^{2+} molar ratio is less than 1 (Fig. 9*E*). At Ca^{2+}/Mg^{2+} ratios greater than or equal to 1, a new downfield peak appears at 10.18 ppm assigned to Gly-40 that represents Ca^{2+} binding at EF-1 (Fig. 9, *E-F*). The lack of a downfield-shifted amide proton resonance for Gly-76 (6-position of EF-2) suggests that neither Ca^{2+} nor Mg^{2+} binds to EF-2, consistent with our Ca^{2+} binding analyses above (Figs. 2 and 3). In summary, EF-3 and EF-4 bind Ca^{2+}, EF-1 binds Mg^{2+}, and EF-2 binds neither Mg^{2+} nor Ca^{2+} under physiological conditions (5 m_M Mg^{2+} and 0.1-10 μ_M Ca^{2+}).

The amide NMR resonances of Gly-40 (EF-1) and Gly-117 were analyzed as a function (EF-3) of the Ca^{2+}/Mg^{2+} ratio to determine the relative binding selectivity of Ca^{2+} *versus* Mg^{2+} (Fig. 10). The intensity profile of the amide resonance representing Gly-40 of Mg^{2+}-bound CaBP1 monitors Mg^{2+} dissociation from EF-1 (*black squares* in Fig. 10*A*), and the intensity profile of the peak at (representing Gly40 of Ca^{2+}-bound CaBP1) monitors Ca^{2+} 10.18 ppm binding to EF-1 (*circles* in Fig. 10*A*). The Mg^{2+} dissociation and Ca^{2+} *open* association curves for EF-1 in Fig. 10*A* intersect at a Ca^{2+}/Mg^{2+} ratio of 1:1, suggesting that EF-1 binds Ca^{2+} and Mg^{2+} with equal selectivity. By contrast, the corresponding Mg^{2+} dissociation and Ca^{2+} association curves for EF-3 in Fig. 10*B* intersect at a Ca^{2+}/Mg^{2+} ratio of much less than 1, suggesting that EF-3 binds Ca^{2+} with more than 10-fold selectivity over Mg^{2+}.

DISCUSSION

In this study, we characterized the structural properties of Mg^{2+} and Ca^{2+} binding to the individual EF-hands of recombinant human CaBP1. Mg^{2+} binds constitutively to EF-1 under physiological conditions, Ca^{2+} binds functionally to EF-3 and EF-4, and neither Ca^{2+} nor Mg^{2+} binds to EF-2. The lack of Ca^{2+} binding to EF-2 is most likely the result of having Gly-75 at the 5-position of the EF-hand loop (Fig. 1), which lacks an oxygen-containing side chain needed for chelating Ca^{2+}. Glycine at this position is conserved in the other CaBP members, implying that EF-2 must be disabled in the other family members as well. Our NMR analysis reveals that Mg^{2+} binding to CaBP1 induces a global conformational change throughout the protein, whereas Ca^{2+} induces localized conformational changes in EF-3 and EF-4. Mg^{2+} and Ca^{2+} cause distinct conformational changes that dramatically increase folding stability and promote protein dimerization. We propose that CaBP1 switches between structurally distinct Mg^{2+}-bound and Ca^{2+}-bound states under physiological conditions. These conformational states may play a role in the regulation of Ca^{2+} channels and other target proteins.

Constitutive Mg^{2+} Binding—The first EF-hand (EF-1) of CaBP1 binds Ca^{2+} with relatively low affinity (Fig. 2) and without selectivity over Mg^{2+} (Fig. 10*A*). As a consequence, EF-1 must be bound to Mg^{2+} and not Ca^{2+} under physiological conditions (0.1-10 μ_M Ca^{2+} and 5 m_M Mg^{2+}). The low Ca^{2+} affinity and loss of Ca^{2+} selectivity is likely due to Asp-46 instead of Glu at the 12-position of the binding loop in EF-1 (Fig. 1). Other EF-hand proteins like DREAM (29), myosin light chain (28), sarcoplasmic calcium-binding protein (52), and CIB (30) contain Asp at the 12-position of particular EF-hands and also exhibit a similar loss of Ca^{2+} selectivity. CaBP5 also contains Asp at the 12-position of EF-1, but curiously other CaBP members (*e.g.* CaBP2 and CaBP4) contain Glu (Fig. 1).

Glutamate at the 12-position of the EF-hand binding loop promotes high affinity and selective Ca^{2+} binding (28). The long side chain of glutamate places the carboxylate group close to the bound metal, enabling it to serve as a bidentate ligand that forms two coordinate covalent bonds

NIH-PA Author Manuscript

NIH-PA Author Manuscript

NIH-PA Author Manuscript

with Ca^{2+}, as seen in crystal structures of many EF-hand proteins (18,19,53,54). The bidentate interaction is critical for forming a pentagonal bipyramidal ligand geometry around the bound Ca^{2+}, in contrast to an octahedral ligand geometry favored by Mg^{2+}. Hence, the bidentate interaction within the EF-hand has been postulated to be important for conferring Ca^{2+}-binding specificity with high affinity (28,55).

Replacing glutamate with aspartate at the 12-position lowers the Ca^{2+} binding affinity and selectivity as evidenced by EF-1 (Figs. 2 and 10). The low Ca^{2+} affinity may be the result of the shorter Asp side chain that places the carboxylate group further away from the bound metal. The shorter Asp side chain at the 12-position may also allow space for the binding of hydrated Mg^{2+} species, which is sterically forbidden by Glu at the 12-position. The dehydration energy of Mg^{2+} is much higher than that of Ca^{2+} (56-58). Normally, Ca^{2+} binds favorably to an EF-hand by shedding its bound water molecules, whereas Mg^{2+} remains hydrated and binds less favorably. Replacing Glu with Asp at the 12-position may increase the relative affinity for Mg^{2+} by permitting the binding of partially hydrated species. To summarize, an important structural determinant for metal binding selectivity of the EF-hand is the type of acidic side chain at the 12-position (Glu *versus* Asp) that can discriminate the different coordination number for Ca^{2+} *versus* Mg^{2+} (7 *versus* 6) and/or their different hydration energetics.

Differential Regulation of Ca^{2+} Channels by CaBP1 and Calmodulin—CaBP1 and calmodulin (CaM) both bind to L-type ($Ca_V1.2$) Ca^{2+} channels and differentially regulate channel activity (14). CaM binds constitutively to $Ca_V1.2$ and causes Ca^{2+}-induced channel closure (59), whereas CaBP1 promotes channel opening (15). This antagonism may be explained in part by structural differences between CaBP1 and CaM. In this study we demonstrate that CaBP1 forms a dimer in solution in contrast with the monomeric structure of calmodulin. The dimeric structure of CaBP1 unfolds in one cooperative step (Fig. 5), suggesting that the two domains of CaBP1 may be structurally associated with each other, unlike the two noninteracting domains of CaM (45,60). Another structural difference is that CaM binds four Ca^{2+}, whereas CaBP1 binds functionally to only two Ca^{2+} at EF-3 and EF-4. CaM mutants that lack Ca^{2+} binding to EF-1 and EF-2 have very different functional properties compared with wild type (61,62). Hence, the lack of Ca^{2+} binding to EF-1 and EF-2 of CaBP1 may be responsible for conferring its functional differences with CaM. Finally, CaPB1 binds constitutively to Mg^{2+} at EF-1 as described above, whereas CaM does not. Taken together, these structural differences may help to understand how CaBP1 and CaM differentially regulate $Ca_V1.2$ channels.

Implications for Target Recognition—Both Mg^{2+}-bound and Ca^{2+}-bound forms of CaBP1 were shown in this study to have stable tertiary structures, and both forms bind to Ca^{2+} channels (11-14). We propose that constitutive Mg^{2+} binding may be necessary for stabilizing the interaction of CaBP1 with protein targets in the absence of Ca^{2+}. Mg^{2+} also stabilizes the tertiary structure of other EF-hand proteins such as GCAP-2 (32), myosin light chain (28), CIB (30), and DREAM (29) that similarly interact with protein or DNA targets in the absence of Ca^{2+}. Ca^{2+}-induced conformational changes in CaBP1 are localized to residues in the C-terminal domain (EF-3 and EF-4), implicating the C-terminal residues in making Ca^{2+}-dependent contacts with the Ca^{2+} channel. By contrast, the N-terminal domain of CaBP1 does not change structure in response to Ca^{2+} binding, suggesting that N-terminal residues constitutively interact with the Ca^{2+} channel. Such an interaction may help explain the observation that CaBP1 binds to $InsP_3R$ even in the absence of Ca^{2+} (11,12).

CaBP1 forms a protein dimer in solution that may be functionally important for channel regulation. We propose that a pair of CaBP1 dimers might come together at the cytosolic surface of the tetrameric InsP3R Ca^{2+} channel to form a 4-fold symmetric complex. Such a cytosolic interaction would allow CaBP1 to function like an iris in front of the channel pore and thereby modulate the passage of Ca^{2+} through the channel. Ca^{2+}-induced conformational

NIH-PA Author Manuscript
NIH-PA Author Manuscript
NIH-PA Author Manuscript

changes to CaBP1 might serve to constrict the "iris" and block the pore, which could explain the reduced Ca^{2+} permeability of $InsP_3R$ at high cytosolic Ca^{2+} levels (12). In addition, CaBP1 may induce allosteric changes within the channel protein that would indirectly control channel activity. Indeed, CaBP1 has been shown recently to interact with the regulatory N-terminal domain of both $InsP_3R$ (12,63) and L-type Ca^{2+} channels (14). In the future, we plan to determine at atomic resolution the Ca^{2+}-induced structural changes of CaBP1 and its interaction with target proteins in order to describe more thoroughly how CaBP1 modulates the activity of Ca^{2+} channels.

Acknowledgements

Acknowledgments—We thank Fred Schwarz and Nese Sari for help with calorimetry and NMR experiments.

REFERENCES

1. Haeseleer F, Sokal I, Verlinde CL, Erdjument H, Tempst P, Pronin AN, Benovic JL, Fariss RN, Palczewski K. J. Biol. Chem 2000;275:1247–1260. [PubMed: 10625670]
2. Haeseleer F, Imanishi Y, Sokal I, Filipek S, Palczewski K. Biochem. Biophys. Res. Commun 2002;290:615–623. [PubMed: 11785943]
3. Ikura M. Trends Biochem. Sci 1996;21:14–17. [PubMed: 8848832]
4. Moncrief ND, Kretsinger RH, Goodman M. J. Mol. Evol 1990;30:522–562. [PubMed: 2115931]
5. Palczewski K, Polans AS, Baehr W, Ames JB. BioEssays 2000;22:337–350. [PubMed: 10723031]
6. Haynes LP, Tepikin AV, Burgoyne RD. J. Biol. Chem 2004;279:547–555. [PubMed: 14570872]
7. Menger N, Seidenbecher CI, Gundelfinger ED, Kreutz MR. Cell Tissue Res 1999;298:21–32. [PubMed: 10555536]
8. Seidenbecher CI, Langnaese K, Sanmarti L, Boeckers TM, Smalla KH, Sabel BA, Garner CC, Gundelfinger ED, Kreutz MR. J. Biol. Chem 1998;273:21324–21331. [PubMed: 9694893]
9. Seidenbecher CI, Reissner C, Kreutz MR. Adv. Exp. Med. Biol 2002;514:451–463. [PubMed: 12596938]
10. Laube G, Seidenbecher CI, Richter K, Dieterich DC, Hoffmann B, Landwehr M, Smalla KH, Winter C, Bockers TM, Wolf G, Gundelfinger ED, Kreutz MR. Mol. Cell. Neurosci 2002;19:459–475. [PubMed: 11906216]
11. Yang, J.; McBride, S.; Mak, DO.; Vardi, N.; Palczewski, K.; Haeseleer, F.; Foskett, JK. Proc. Natl. Acad. Sci.; U. S. A.. 2002. p. 7711-7716.
12. Kasri NN, Holmes AM, Bultynck G, Parys JB, Bootman MD, Rietdorf K, Missiaen L, McDonald F, De Smedt H, Conway SJ, Holmes AB, Berridge MJ, Roderick HL. EMBO J 2004;23:312–321. [PubMed: 14685260]
13. Lee A, Westenbroek RE, Haeseleer F, Palczewski K, Scheuer T, Catterall WA. Nat. Neurosci 2002;5:210–217. [PubMed: 11865310]
14. Zhou H, Yu K, McCoy KL, Lee A. J. Biol. Chem 2005;280:29612–29619. [PubMed: 15980432]
15. Zhou H, Kim SA, Kirk EA, Tippens AL, Sun H, Haeseleer F, Lee A. J. Neurosci 2004;24:4698–4708. [PubMed: 15140941]
16. Kinoshita-Kawada M, Tang J, Xiao R, Kaneko S, Foskett JK, Zhu MX. Pfluegers Arch 2005;450:345–354. [PubMed: 15895247]
17. Haeseleer F, Imanishi Y, Maeda T, Possin DE, Maeda A, Lee A, Reike F, Palczewski K. Nat. Neurosci 2004;7:1079–1087. [PubMed: 15452577]
18. Babu YS, Bugg CE, Cook WJ. J. Mol. Biol 1988;204:191–204. [PubMed: 3145979]
19. Flaherty KM, Zozulya S, Stryer L, McKay DB. Cell 1993;75:709–716. [PubMed: 8242744]
20. Ames JB, Ishima R, Tanaka T, Gordon JI, Stryer L, Ikura M. Nature 1997;389:198–202. [PubMed: 9296500]
21. Ames JB, Dizhoor AM, Ikura M, Palczewski K, Stryer L. J. Biol. Chem 1999;274:19329–19337. [PubMed: 10383444]

NIH-PA Author Manuscript

NIH-PA Author Manuscript

NIH-PA Author Manuscript

22. Ames JB, Hendricks KB, Strahl T, Huttner IG, Hamasaki N, Thorner J. Biochemistry 2000;39:12149–12161. [PubMed: 11015193]
23. Burgoyne RD, Weiss JL. Biochem. J 2001;353:1–12. [PubMed: 11115393]
24. Bourne Y, Dannenberg J, Pollmann VV, Marchot P, Pongs O. J. Biol. Chem 2001;276:11949–11955. [PubMed: 11092894]
25. Vijay-Kumar S, Kumar VD. Nat. Struct. Biol 1999;6:80–88. [PubMed: 9886296]
26. Zhou W, Qian Y, Kunjilwar K, Pfaffinger PJ, Choe S. Neuron 2004;41:573–586. [PubMed: 14980206]
27. Linse S, Helmersson A, Forsen S. J. Biol. Chem 1991;266:8050–8054. [PubMed: 1902469]
28. da Silva AC, Kendrick-Jones J, Reinach FC. J. Biol. Chem 1995;270:6773–6778. [PubMed: 7896823]
29. Osawa M, Dace A, Tong KI, Valiveti A, Ikura M, Ames JB. J. Biol. Chem 2005;280:18008–18014. [PubMed: 15746104]
30. Yamniuk AP, Nguyen LT, Hoang TT, Vogel HJ. Biochemistry 2004;43:2558–2568. [PubMed: 14992593]
31. Brocard JB, Rajdev S, Reynolds IJ. Neuron 1993;11:751–757. [PubMed: 8104432]
32. Peshenko IV, Dizhoor AM. J. Biol. Chem 2004;279:16903–16906. [PubMed: 14993224]
33. Cox JA, Durussel I, Comte M, Nef S, Nef P, Lenz SE, Gundelfinger ED. J. Biol. Chem 1994;269:32807–32813. [PubMed: 7806504]
34. Ames JB, Hamasaki N, Molchanova T. Biochemistry 2002;41:5776–5787. [PubMed: 11980481]
35. Paulus H. Anal. Biochem 1969;32:91–100. [PubMed: 5398270]
36. Hendricks KB, Wang BQ, Schnieders EA, Thorner J. Nat. Cell Biol 1999;1:234–241. [PubMed: 10559922]
37. Chakrabarti MC, Schwarz FP. Nucleic Acids Res 1999;27:4801–4806. [PubMed: 10572181]
38. Schwarz FP, Puri KD, Bhat RG, Surolia A. J. Biol. Chem 1993;268:7668–7677. [PubMed: 8463297]
39. Wiseman T, Williston S, Brandts JF, Lin LN. Anal. Biochem 1989;179:131–137. [PubMed: 2757186]
40. Papish AL, Tari LW, Vogel HJ. Biophys. J 2002;83:1455–1464. [PubMed: 12202371]
41. Clore GM, Gronenborn AM. Nat. Struct. Biol 1997;4:849–853. [PubMed: 9377157]
42. Henzl MT, Larson JD, Agah S. Anal. Biochem 2003;19:216–233. [PubMed: 12871715]
43. Gilli R, Lafitte D, Lopez C, Kilhoffer M, Makarov A, Briand C, Haiech J. Biochemistry 1998;37:5450–5456. [PubMed: 9548926]
44. Biekofsky RR, Martin SR, McCormick JE, Masino L, Fefeu S, Bayley PM, Feeney J. Biochemistry 2002;41:6850–6859. [PubMed: 12022890]
45. Masino L, Martin SR, Bayley PM. Protein Sci 2000;9:1519–1529. [PubMed: 10975573]
46. Tsalkova TN, Privalov PL. J. Mol. Biol 1985;181:533–544. [PubMed: 3999139]
47. McCubbin WD, Hincke MT, Kay CM. Can. J. Biochem 1980;58:683–691. [PubMed: 7459693]
48. Yang C, Jas GS, Kuczera K. J. Biomol. Struct. Dyn 2001;19:247–271. [PubMed: 11697730]
49. Gombos Z, Durussel I, Ikura M, Rose DR, Cox JA, Chakrabarti A. Biochemistry 2003;42:5531–5539. [PubMed: 12731896]
50. Qi XF, Bagby S, Gombos Z, Ikura M, Chakrabarti A. Eur. J. Biochem 2001;268:4653–4663. [PubMed: 11532002]
51. Altieri AS, Hinton DP, Byrd RA. J. Am. Chem. Soc 1995;117:7566–7567.
52. Wnuk W, Cox JA, Kohler LG, Stein EA. J. Biol. Chem 1979;254:5284–5289. [PubMed: 447649]
53. Herzberg O, James MN. J. Mol. Biol 1988;203:761–779. [PubMed: 3210231]
54. Vijay-Kumar S, Cook WJ. J. Mol. Biol 1992;224:413–426. [PubMed: 1560459]
55. Snyder EE, Buoscio BW, Falke JJ. Biochemistry 1990;29:3937–3943. [PubMed: 2162201]
56. Eigen M, Hammes GG. Adv. Enzymol. Relat. Areas Mol. Biol 1963;25:1–38. [PubMed: 14149678]
57. Sussman F, Weinstein H. Proc. Natl. Acad. Sci. U. S. A 1989;86:7880–7884. [PubMed: 2813364]
58. Rashin AA, Honig B. J. Phys. Chem 1985;89:5588–5593.
59. Zuhlke RD, Pitt GS, Deisseroth K, Tsien RW, Reuter H. Nature 1999;399:159–162. [PubMed: 10335846]

NIH-PA Author Manuscript

NIH-PA Author Manuscript

NIH-PA Author Manuscript

60. Strynadka NC, James MN. Proteins 1988;3:1–17. [PubMed: 3375233]
61. Gao ZH, Krebs J, VanBerkum MF, Tang WJ, Maune JF, Means AR, Stull JT, Beckingham K. J. Biol. Chem 1993;268:20096–20104. [PubMed: 8376368]
62. Stevens-Truss R, Beckingham K, Marletta MA. Biochemistry 1997;36:12337–12345. [PubMed: 9315874]
63. Bosanac I, Yamazaki H, Matsu-Ura T, Michikawa T, Mikoshiba K, Ikura M. Mol. Cell 2005;17:193–203. [PubMed: 15664189]

NIH-PA Author Manuscript

NIH-PA Author Manuscript

NIH-PA Author Manuscript

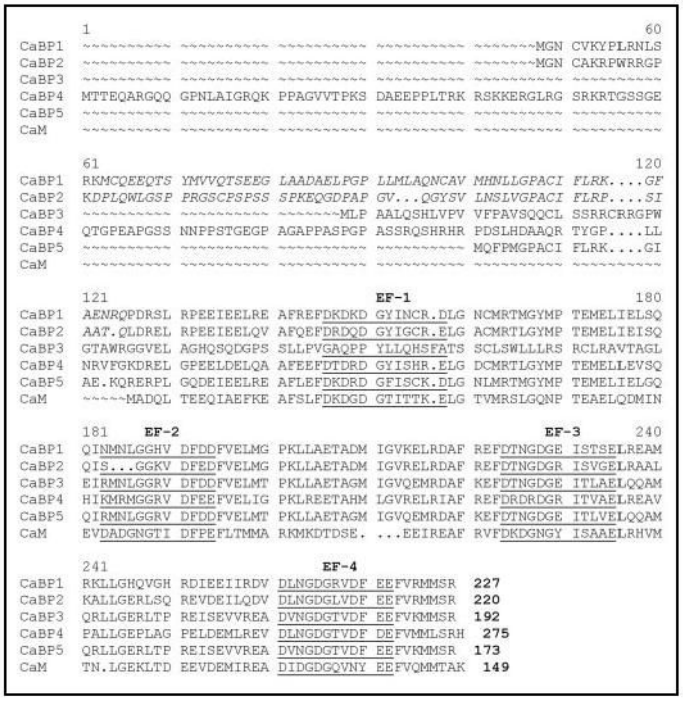

FIGURE 1.

Alignment of amino acid sequence of human CaBP1 with those of calmodulin and other members of the neuron-specific CaBP sub-branch of the EF-hand superfamily. The Ca^{2+} binding loops of the four EF-hands are *underlined*. The sequences of long splice variants of CaBP1 and CaBP2 (as defined in Ref. 1) are shown. Short splice variants lack the italicized residues.

NIH-PA Author Manuscript

NIH-PA Author Manuscript

NIH-PA Author Manuscript

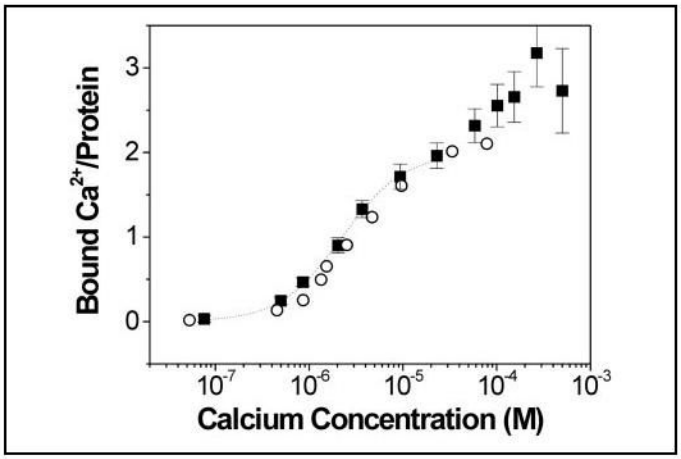

FIGURE 2.

Equilibrium Ca^{2+} binding to CaBP1. Titrations of $^{45}Ca^{2+}$ binding to CaBP1 were conducted using an ultrafiltration method, as described under "Experimental Procedures." Number of ions bound per protein is plotted as a function of the free calcium concentration. Binding data measured in the absence and presence of 5 mM Mg^{2+} are indicated by *black squares* and *open circles*, respectively. The *solid line* represents the best fit to the Hill model using parameters as defined in the text, K_d = 2.5 μM and Hill coefficient of 1.3.

NIH-PA Author Manuscript
NIH-PA Author Manuscript
NIH-PA Author Manuscript

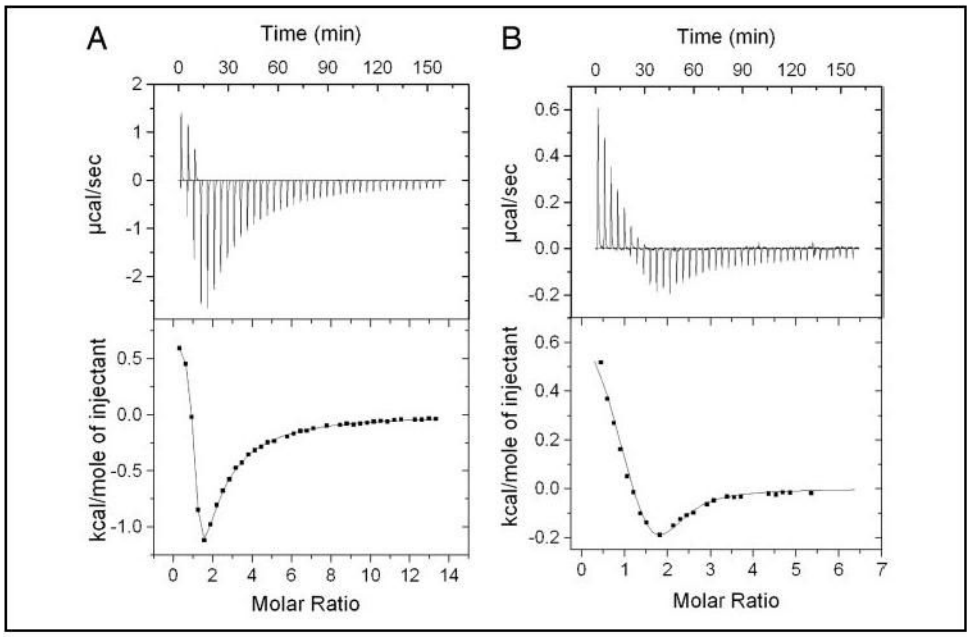

FIGURE 3.

Isothermal titration microcalorimetric analysis of Ca^{2+} binding to apo- (*A*) and Mg^{2+}-bound (*B*) CaBP1. Trace of the calorimetric titration of 40× 5-µl aliquots of 15 mM $CaCl_2$ into 180 µM CaBP1 (*A*) or 5 mM $CaCl_2$ into 120 µM CaBP1 (*B*) (*top*), and integrated binding isotherms (*bottom*). *Solid lines* represent the best fit to sequential sites model in *A*, where $K_1 = 4 \times 10^5$ M^{-1}, $\Delta H_1 = 0.703 \pm 0.012$ kcal/mol, $K_2 = 3019$ M^{-1}, and $\Delta H_2 = -8.14$ kcal/mol; and in *B* where $K_1 = 4 \times 10^5$ M^{-1}, $\Delta H_1 = 0.611$ kcal/mol, $K_2 = 5 \times 10^4$ M^{-1}, and $\Delta H_2 = -0.531$ kcal/mol.

NIH-PA Author Manuscript

NIH-PA Author Manuscript

NIH-PA Author Manuscript

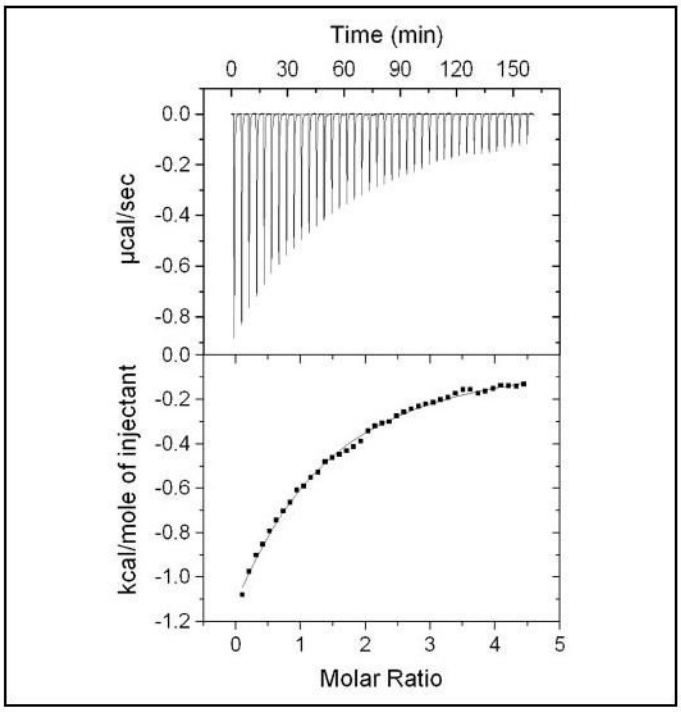

FIGURE 4.

Isothermal titration microcalorimetric analysis of the Mg^{2+} binding to CaBP1. Trace of the calorimetric titration of 40× 5-µl aliquots of 15.0 mM $MgCl_2$ into the cell containing 172 µM apoCaBP1 (*top*) and integrated binding isotherm (*bottom*). The binding isotherm was fit using a 1-site model where K_1 = 3329 M^{-1} and ΔH_1 =-3.725 kcal/mol^{-1}.

NIH-PA Author Manuscript
NIH-PA Author Manuscript
NIH-PA Author Manuscript

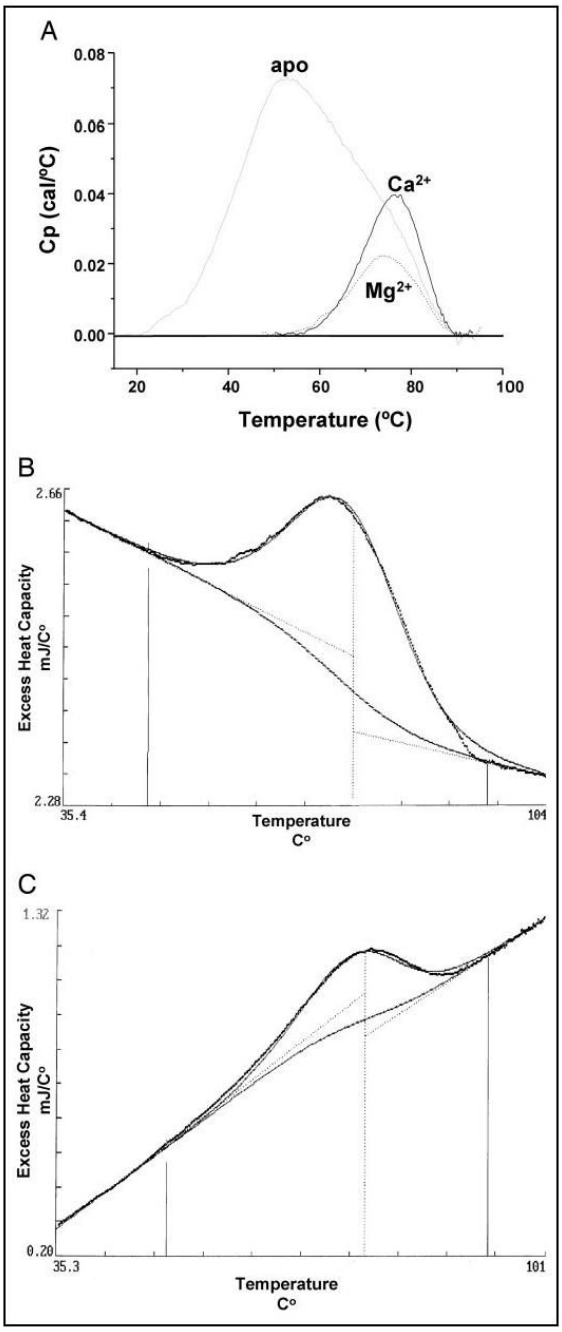

FIGURE 5.

Differential scanning calorimetric analysis of protein unfolding of CaBP1. *A*, overlay of DSC scans of apo-, Ca^{2+}-bound, and Mg^{2+}-bound CaBP1. The protein concentration was 126 μM in 20 mM Tris buffer, pH 7.5, containing 0.1 M KCl, 1 mM DTT supplemented with either 5 mM EGTA (apo-), 5 mM MgCl (Mg^{2+}-bound), or 5 mM $CaCl_2$ (Ca^{2+}-bound). The scan rate was 60 K/h^{-1}, and the cell volume was 0.511 ml. A two-state transition model (B → 2A) was fit to DSC scans of Mg^{2+}-bound (*B*) and Ca^{2+}-bound (*C*) CaBP1 as indicated by *dotted lines*. The fitting parameters were ΔH_v = 287/341 cal/mol, ΔC_p =-5.8/-12 kJ/°C, and T_m = 76.57/76.82 °C in *B* and *C*, respectively.

NIH-PA Author Manuscript

NIH-PA Author Manuscript

NIH-PA Author Manuscript

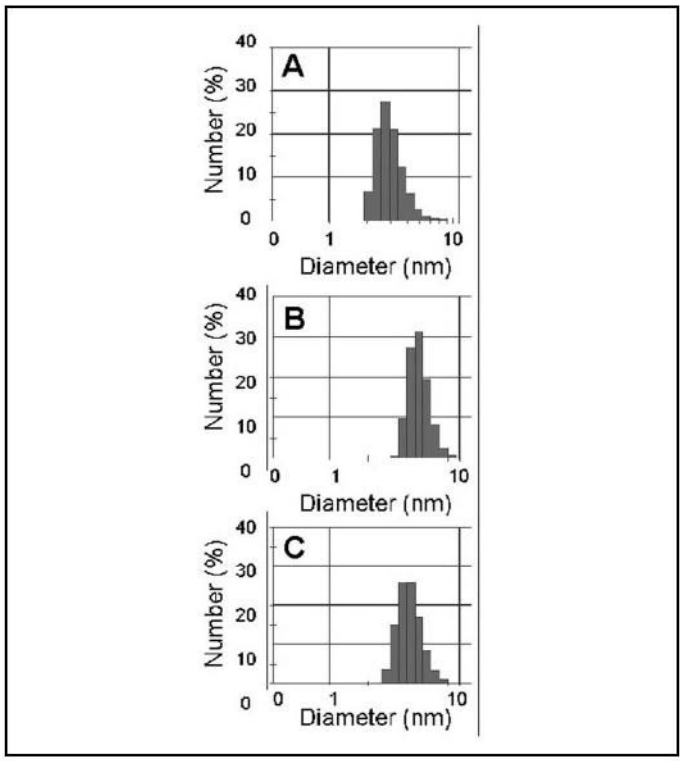

FIGURE 6.

Dynamic light scattering size distribution histogram for apo- (*A*), Mg^{2+}-bound (*B*), and Ca^{2+}-bound (*C*) CaBP1. The median hydrodynamic diameter (and polydispersity) is 2.7 nm (40%), 4.8 nm (20%), and 4.2 nm (25%) for apo-, Mg^{2+}-bound, and Ca^{2+}-bound CaBP1, respectively.

NIH-PA Author Manuscript
NIH-PA Author Manuscript
NIH-PA Author Manuscript

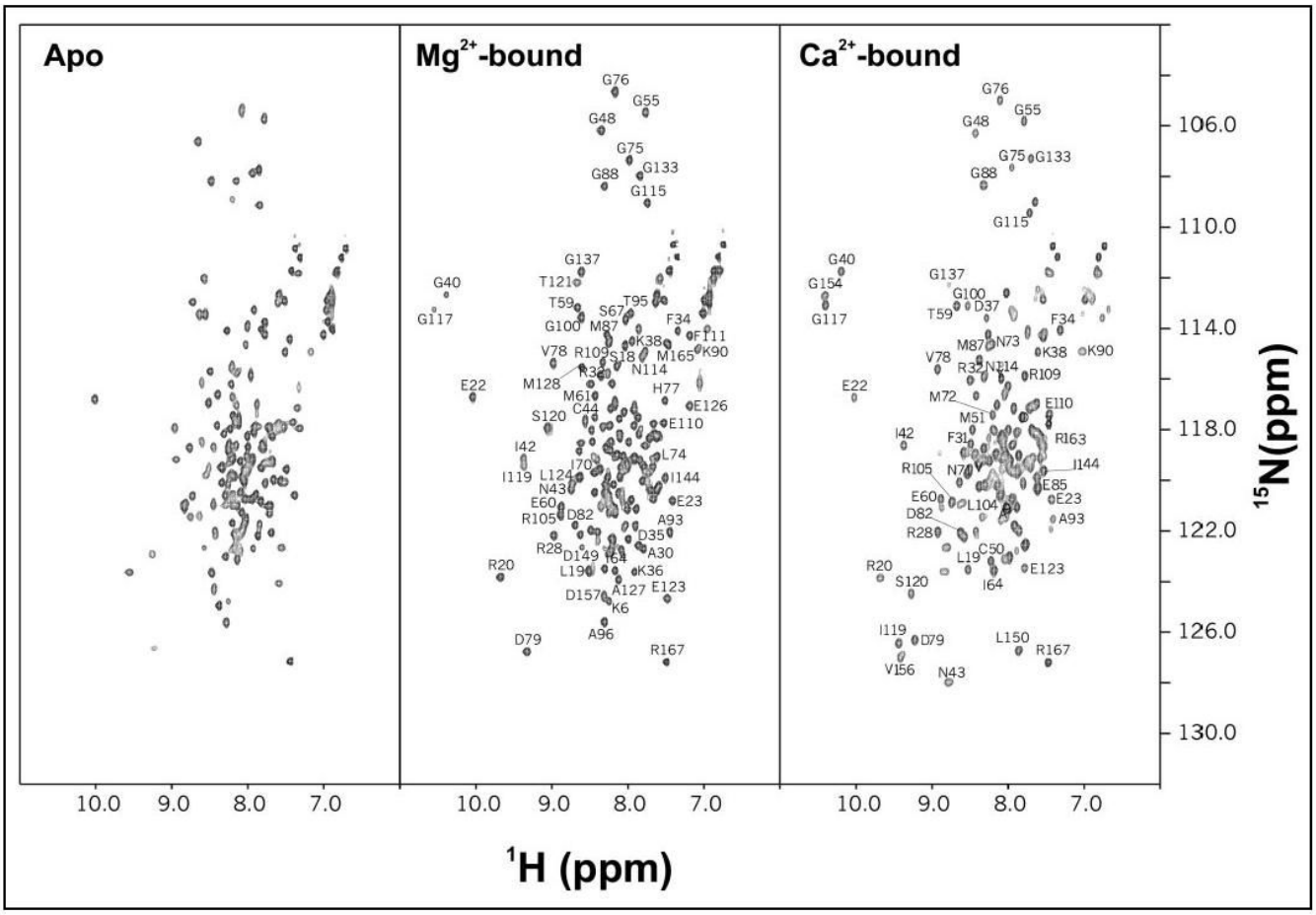

FIGURE 7.

Two-dimensional ^{15}N-^{1}H HSQC NMR spectra of apo- (*left panel*), Mg^{2+}-bound (*middle panel*), and Ca^{2+}-bound (*right panel*) CaBP1. Each protein sample was uniformly labeled with nitrogen-15, and spectra were recorded at 600-MHz ^{1}H frequency.

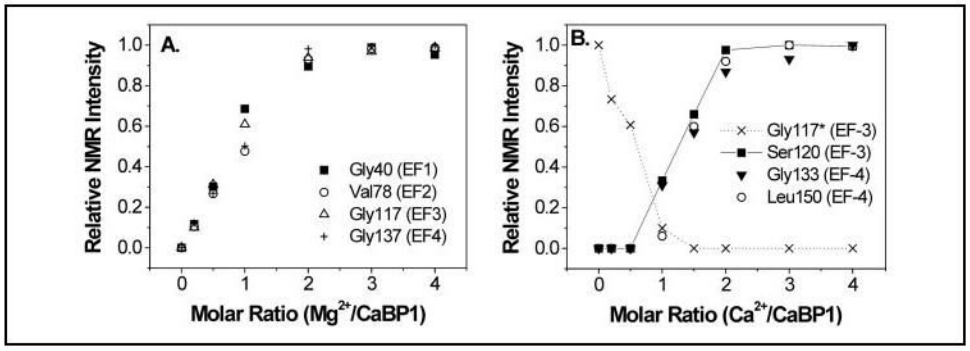

FIGURE 8.

Relative NMR intensities of selected amide resonances from Fig. 7 plotted as a function of Mg^{2+} (*A*) and Ca^{2+} concentration (*B*).

NIH-PA Author Manuscript NIH-PA Author Manuscript NIH-PA Author Manuscript

NIH-PA Author Manuscript

NIH-PA Author Manuscript

NIH-PA Author Manuscript

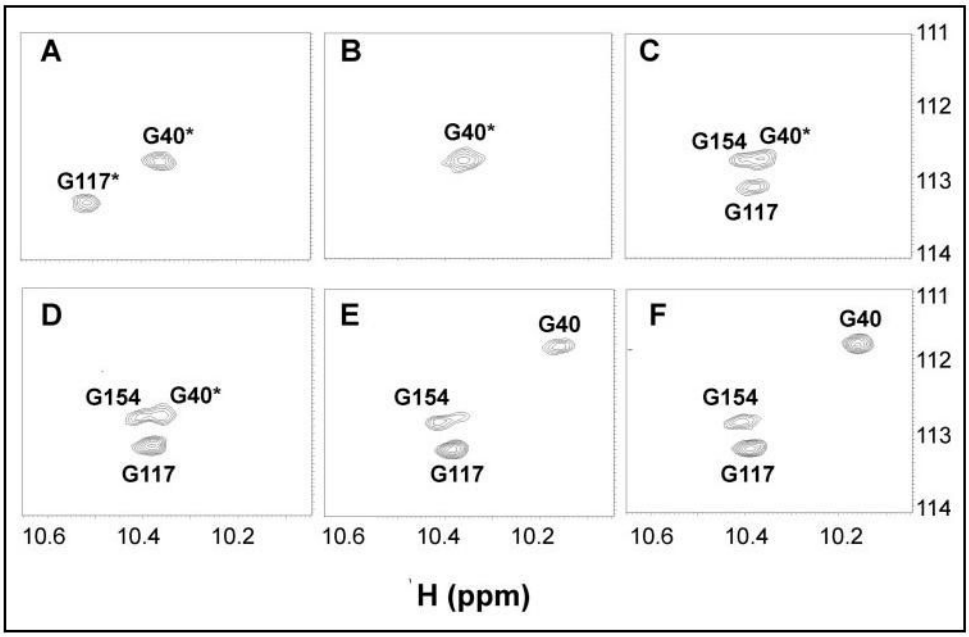

FIGURE 9.

Downfield spectral region of ^{15}N-^{1}H HSQC NMR spectra of CaBP1 (200 μM) recorded as a function of increasing Ca^{2+} concentration in the presence of physiological Mg^{2+} (5 mM). The molar ratio of Ca^{2+}/Mg^{2+} and {Ca^{2+}/protein} in each case was 0.0 {0.0} (*A*), 0.04 {1.0} (*B*), 0.08 {2.0} (*C*), 0.16 {4.0} (*D*), 1.0 {25} (*E*), and 2.0 {50} (*F*). *Asterisk* indicates amide resonances assigned to Mg^{2+}-bound CaBP1.

NIH-PA Author Manuscript
NIH-PA Author Manuscript
NIH-PA Author Manuscript

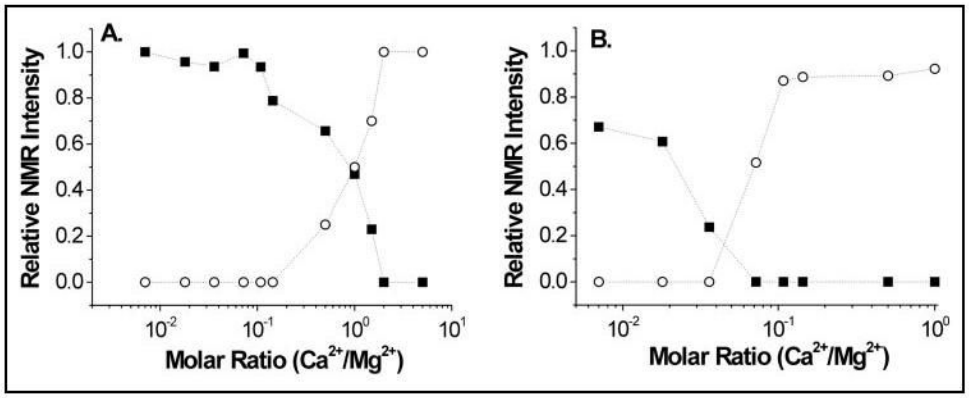

FIGURE 10.

Relative NMR intensities of amide resonances assigned to Gly-40 (*A*) and Gly-117 (*B*) plotted as a function of increasing Ca^{2+} concentration in the presence of physiological Mg^{2+}. The intensities of amide resonances at 10.35 ppm (Gly-40) and 10.52 ppm (Gly-117) of Mg^{2+}-bound CaBP1 (*black squares*) represent concentration profiles that monitor Mg^{2+} dissociation from EF-1 and EF-3, respectively, in *A* and *B*. Intensities of resonances at 10.18 ppm (Gly-40) and 10.38 ppm (Gly-117) of Ca^{2+}-bound CaBP1 (*open circles*) represent concentration profiles that monitor Ca^{2+} association to EF-1 and EF-3, respectively.